sensors

MDPI

Article

Highly Sensitive and Selective Defect WS_2 Chemical Sensor for Detecting HCHO Toxic Gases

Zhen Cui [1,2,*], Hanxiao Wang [1], Kunqi Yang [1], Yang Shen [1], Ke Qin [1], Pei Yuan [1] and Enling Li [1,*]

[1] School of Science, Xi'an University of Technology, Xi'an 710054, China; 2220920058@stu.xaut.edu.cn (H.W.); 2210920050@stu.xaut.edu.cn (K.Y.); shenyang@xaut.edu.cn (Y.S.); 2220920069@stu.xaut.edu.cn (K.Q.); 2220920057@stu.xaut.edu.cn (P.Y.)

[2] School of Automation and Information Engineering, Xi'an University of Technology, Xi'an 710048, China

* Correspondence: zcui@xaut.edu.cn (Z.C.); lienling@xaut.edu.cn (E.L.)

Abstract: The gas sensitivity of the W defect in WS_2 (V_W/WS_2) to five toxic gases—HCHO, CH_4, CH_3HO, CH_3OH, and CH_3CH_3—has been examined in this article. These five gases were adsorbed on the V_W/WS_2 surface, and the band, density of state (DOS), charge density difference (CDD), work function (*W*), current–voltage (I–V) characteristic, and sensitivity of adsorption systems were determined. Interestingly, for HCHO-V_W/WS_2, the energy level contribution of HCHO is closer to the Fermi level, the charge transfer (*B*) is the largest (0.104 e), the increase in *W* is more obvious than other adsorption systems, the slope of the I–V characteristic changes more obviously, and the calculated sensitivity is the highest. To sum up, V_W/WS_2 is more sensitive to HCHO. In conclusion, V_W/WS_2 has a great deal of promise for producing HCHO chemical sensors due to its high sensitivity and selectivity for HCHO, which can aid in the precise and efficient detection of toxic gases.

Keywords: defect WS_2 chemical sensors; sensitivity; selectivity; toxic gases

check for updates

Citation: Cui, Z.; Wang, H.; Yang, K.; Shen, Y.; Qin, K.; Yuan, P.; Li, E. Highly Sensitive and Selective Defect WS_2 Chemical Sensor for Detecting HCHO Toxic Gases. *Sensors* **2024**, *24*, 762. https://doi.org/10.3390/s24030762

Academic Editors: Marijo Buzuk, Maša Buljac and Nives Vladislavić

Received: 27 December 2023
Revised: 14 January 2024
Accepted: 17 January 2024
Published: 24 January 2024

1. Introduction

The majority of volatile organic compounds (VOCs) such as HCHO, CH_4, CH_3CHO, CH_3OH, and CH_3CH_3 are hazardous to human health and safety, the environment, and cause cancer [1]. In order to identify harmful gases and lessen their damage, we need devices. Chemical sensors are commonly used to detect and analyze chemical substances and can measure the existence and specific concentration of experimental substances. Researchers have been continuously exploring and innovating chemical sensors to address the issue of harmful gas detection and monitoring in various domains.

In the current period of rapid scientific and technological advancement, chemical sensors are progressively becoming essential instruments across a wide range of fields. These sensors have the ability to detect sensitive signals and accurately identify chemicals, thus affecting our life, health, and environment. For instance, the use of chemical sensors is significant in the field of environmental protection. A number of toxic gases, including CO and SO_2, are present in the atmosphere and are extremely dangerous to both human health and the environment. Scientists can track and identify the concentration of these dangerous gases in real time and take appropriate action to protect the environment by inventing high-performance chemical sensors. Furthermore, the use of chemical sensors in the industrial sector is very important. Consider a chemical plant as an example. During the production process, several hazardous gases are emitted, including H_2S and NH_3. High-performance chemical sensors allow workers to detect and identify the presence of dangerous gases in real time, allowing them to avoid potential hazards that could endanger their health. Furthermore, the medical industry is also involved in the application of chemical sensors. For instance, certain harmful gases, such as NO, will be created during respiratory therapy and will negatively affect the health of patients. Medical personnel can monitor the concentration of these dangerous gases in real time and take appropriate action

to safeguard patients' respiratory systems by employing chemical sensors with excellent sensitivity and selectivity.

To put it succinctly, chemical sensors are crucial for the identification and tracking of toxic gases. Continuous research and innovation can enhance the dependability, sensitivity, and accuracy of chemical sensors.

Chemical sensors have been designed using nanomaterials on a large scale in recent years due to the advancement of nanotechnology [2–4]. Chemical sensors' performance has been greatly enhanced using nanomaterials, primarily in the following areas: Increasing specific surface area: in comparison to conventional materials, nanomaterials have a higher specific surface area per unit mass or volume. As a result, nanomaterials can offer more active sites and improve their interaction with target molecules, increasing the sensitivity of the sensor [5]. Enhance conductivity: nanomaterials often exhibit high levels of thermal and electrical conductivity, which helps to enhance sensors' response times and signal conduction efficiency. This holds great significance for instantaneous monitoring and prompt reaction to specific compounds, particularly in the domains of environmental and medical monitoring. Introducing new features: nanomaterials exhibit physical and chemical properties distinct from large-scale materials due to the size effect and quantum effect. New properties, such as optics, electricity, and magnetism, can be added to nanomaterials with great care to improve the sensor's selectivity and reactivity to target molecules. Boost stability and durability: the high surface area and unique structure of nanomaterials contribute to the sensors' increased stability and durability. Realizing multifunctional design: By mixing several nanomaterial types, chemical sensors with multifunctional capabilities can be designed thanks to the multifunctional nature of nanomaterials. This multifunctional architecture enhances the sensor's overall performance by simultaneously detecting numerous target molecules. As a result, the introduction of nanomaterials opens up new avenues for chemical sensor design.

Chemical sensors have advanced quickly in the last few years, but there are still a lot of restrictions. Certain chemical sensors can produce erroneous measurement findings due to cross-sensitivity to toxic gases, which occurs when other gases interfere with the sensor [6]. Different chemical sensors have varying degrees of stability and accuracy, and some are more sensitive to environmental factors like humidity, temperature, and pressure, which require calibration and adjustment [7–9]. High sensitivity and selectivity are necessary for the sensor to enable effective monitoring, and high performance is required for the detection of toxic gases. Thus, in order to address the needs of toxic gas detection and monitoring in many domains, we should keep researching and developing chemical sensors [10–12].

High-performance gas-sensitive materials must be developed in order to achieve the sensitive detection of toxic gases [13]. Transition metal dichalcogenides [14–16] have a number of superior properties in the realm of chemical sensors, which makes them perfect building blocks for the production of effective sensors. Through the deft application of these properties, we can achieve tremendous gains in sensor performance and design [17–19]. Cui researched how the photoelectric properties of WS_2 and defect for the WS_2 changed when it was adsorbed by CO, NH_3, NO, and NO_2 gas molecules in 2022 [11]. They came to the conclusion that WS_2 is useful for toxic gas detection and gas sensing. WS_2 has a large surface area, active sites, high sensitivity, and controllability, which are beneficial to molecular adsorption and interaction with target molecules, and can achieve highly selective recognition of specific molecules and improve the sensitivity and response speed of the sensor.

On the surface of WS_2 and the W defect for WS_2 V_W/WS_2, we adsorbed HCHO, CH_4, CH_3HO, CH_3OH, and CH_3CH_3, and we computed their electronic properties and work function (W). We selected the V_W/WS_2 adsorption systems to further compute the I–V characteristic and sensitivity since the results were consistent that the electronic properties and W of HCHO-WS_2 and HCHO-V_W/WS_2 changed most obviously in the WS_2 adsorption systems and the V_W/WS_2 adsorption systems [20–22]. We discovered that V_W/WS_2 exhibited excellent sensitivity and selectivity for HCHO. Due to its high sensitivity,

V_W/WS_2 is able to identify toxic gas with a very low concentration of HCHO [23]. Because HCHO is frequently damaging to human health at low concentrations, this is crucial for safeguarding both the environment and people. Second, selectivity refers to V_W/WS_2's ability to recognize variations in various gases and solely react to the toxic gas (HCHO) [24]. Due to these benefits, V_W/WS_2 is a valuable tool for environmental monitoring, industrial safety, and personal safety. It also makes it easier to recognize and manage toxic gases, which is particularly useful for HCHO detection [25].

2. Computational Methods

We calculated the density functional theory (DFT) by using the Vienna ab initio simulation software package 5.4.4 (VASP). The exchange–correlation interaction and the electron–ion interaction are described, respectively, by the extended gradient approximation of Perdew Burke Ernzerhof (PBE) and the projection-enhanced wave approach. In order to assure system stability, we built a 4 × 4 × 1 supercell model and a vacuum layer of 20 Å was added in the z direction for WS_2, defect WS_2, and the adsorption systems. For both structural and electronic structure optimization calculations, the sampling grid in the K space of the Brillouin zone is 9 × 9 × 1, the energy convergence criterion is 10^{-7} eV, the ideal convergence threshold is to guarantee that the force acting on atoms is less than 10^{-3} eV/Å, and the cutoff energy is set to 500 eV.

The adsorption energy (E_{ab}) between molecules was further evaluated. The energy generated when free monolayers combine to form adsorption systems is known as the E_{ab}, and it is expressed as [26–29]:

$$E_{abs} = E_{adsorbedsystem} - \left(E_{monolayer} + E_{targetmolecule}\right) \tag{1}$$

The energy released during the construction of the adsorption system is represented by the symbol E_{abs} in the above equation. The total energy of the adsorption systems is also indicated by the symbol $E_{adsorbedsystem}$. Additionally, the total energy of V_W/WS_2 and gas molecules is indicated by $E_{monolayer}$ and $E_{targetmolecule}$. Lastly, the unit area under consideration is indicated by the sign S.

By utilizing computed differences in charge density difference (CDD) [30] and charge transfer (B) [31], we can analyze the transfer of charges between the adsorption systems. This formula can be expressed as follows:

$$\Delta\rho = \rho_h - \rho_1 - \rho_2 \tag{2}$$

By employing computed variations in charge density (ρ_h, ρ_1, and ρ_2), we can examine the B mechanisms between the V_W/WS_2 and gas molecules. Here, ρ_h represents the charge density of the adsorption systems, while ρ_1 and ρ_2 correspond to the charge densities of the V_W/WS_2 and gas molecules.

We studied the I–V characteristic of the adsorption systems, which was obtained by calculating the current at different bias voltages. The current at a specific bias voltage can be obtained using the following equation [32]:

$$I = \frac{e}{h}\int_{-\infty}^{+\infty} T(E;V_b)[f_L(E;E_F^L - V_b/2) - f_R(E;E_F^R + V_b/2)]\mathrm{d}E \tag{3}$$

where $f_L(E;E_F^L - V_b/2)$, E_F^L, $f_R(E;E_F^R - V_b/2)$, and E_F^R are the Fermi energy level and Fermi distribution at the equilibrium state of the left and right electrodes, respectively. $T(E;V_b)$ is the transmission probability function spectrum for electrons.

Lastly, we used the following formula to evaluate the adsorption systems' sensitivity [33]:

$$S = (G - G_0)/G_0 \times 100\% \tag{4}$$

where G is the conductance of adsorption systems, and G_0 is the conductance of V_W/WS_2.

We used Vienna ab initio simulation package (VASP) software to calculate the electronic properties of the systems, such as energy band, density of state (DOS), CDD, and B, and used Nanodcal 2023A software to calculate the electrical characteristics of I–V [34,35].

3. Results and Discussion

The focus of our research is toxic gases, and HCHO, CH_4, CH_3CHO, CH_3OH, and CH_3CH_3 are the most common toxic gases. There is still a technical gap in the field of detection. So, we adsorbed five gas molecules, HCHO, CH_4, CH_3CHO, CH_3OH, and CH_3CH_3, on WS_2 and optimized their structures. The adsorption distance (H) of the adsorption systems before optimization is 3 Å, the optimized H values are 2.94 Å, 2.80 Å, 2.78 Å, 2.49 Å, and 2.52 Å in Table 1, respectively. We also calculated the E_{ab} of the adsorption systems and determined the most stable model, as shown in Figure 1. Next, the energy bands of the adsorption systems were calculated, as shown in Figure 2. We can see that the energy bands have hardly changed, so the adsorption of gas molecules has little effect on the electronic properties of WS_2. Gas molecules are physically adsorbed. In order to further investigate the physical adsorption of gas molecules, we calculated the DOS; the total DOS of the adsorption system is shown by the gray line in Figure 3, the DOS of WS_2 is represented by the blue line. Compared with the DOS of WS_2, the adsorption systems show a DOS contribution of gas molecules near the Fermi level and the DOS of gas molecules is represented by the red line. The DOS of CH_4 and CH_3CH_3 disappeared near the Fermi level. The DOS of CH_3OH and CH_3CHO is further away from the Fermi level, while the DOS of HCHO is closest to the Fermi level. Therefore, HCHO adsorption has the greatest impact on the electronic properties near the Fermi level compared to other gas adsorption. Figure 4 is the CDD we calculated; the sky-blue area denotes the charge accumulation, and the purple area denotes the charge depletion. The electric field is usually formed by the charge accumulation, and the charge depletion leads to the flow and transport of charges, which in turn affects the electrical characteristics of materials. There is a difference between the energy level of the adsorbed substance and the energy level of the surface, and the movement of electrons leads to the resonance of electrons or the change in local electron density, thus causing B in the adsorption systems. We can see that there is B between the gas molecule and WS_2. In Table 1, combined with the B of the adsorption systems (0.107 e, 0.092 e, 0.088 e, 0.091 e, and 0.089 e, respectively), the B of the HCHO-WS_2 system is the largest, which is consistent with DOS. Next, we calculated the W of the WS_2 adsorption systems, which are 5.72 eV, 5.53 eV, 5.01 eV, 5.15 eV, and 5.53 eV, respectively. Compared with the W of WS_2 (5.39 eV), the W of HCHO-WS_2 increased the most significantly, while the W of CH_3CHO-WS_2 and CH_3OH-WS_2 decreased. The W of CH_4-WS_2 and CH_3CH_3-WS_2 show a slight increase. So, when detecting gas, WS_2 is more likely to react with HCHO. In summary, WS_2 has higher sensitivity and selectivity towards HCHO.

Table 1. The E_{ad}, the H, band gap (E_g), B, and W for WS_2, and HCHO, CH_4, CH_3CHO, CH_3OH, and CH_3CH_3 adsorbed on WS_2.

Configuration	E_{ad} (meV)	H (Å)	E_g (eV)	B (e)	W (eV)	ΔW (eV)
WS_2	-	-	1.775	-	5.39	
HCHO-WS_2	196.72	2.94	1.772	0.107	5.72	0.337
CH_4-WS_2	149.55	2.80	1.772	0.092	5.53	0.140
CH_3CHO-WS_2	233.05	2.78	1.773	0.088	5.01	−0.374
CH_3OH-WS_2	206.27	2.49	1.773	0.091	5.15	−0.232
CH_3CH_3-WS_2	246.02	2.52	1.773	0.089	5.53	0.146

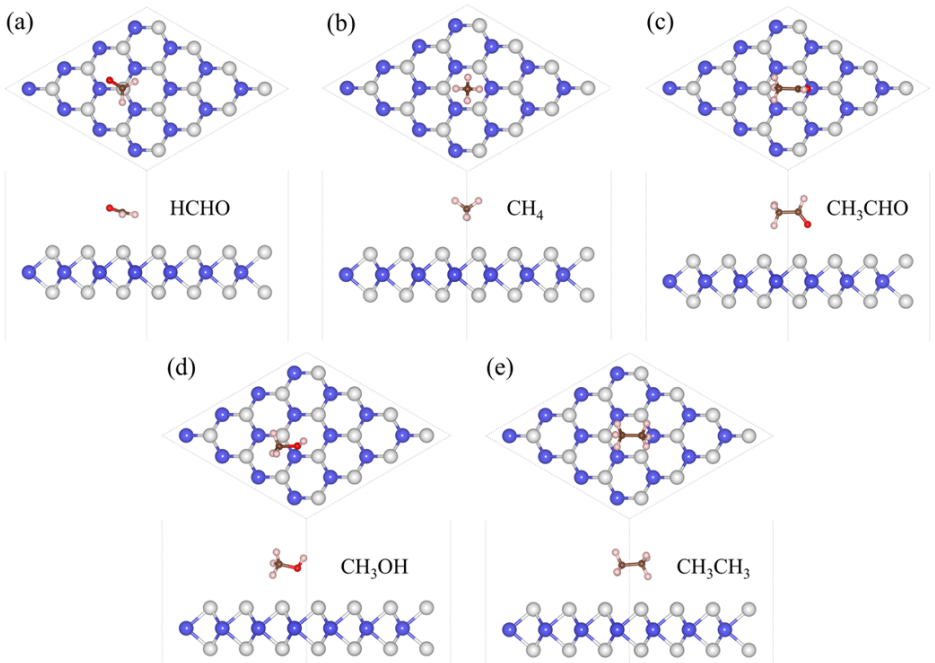

Figure 1. The most stable adsorption configurations of (**a**) HCHO, (**b**) CH_4, (**c**) CH_3CHO, (**d**) CH_3OH, and (**e**) CH_3CH_3 adsorbed on WS_2. The white, blue, brown, pink, and red spheres represent S, W, C, H, and O atoms, respectively.

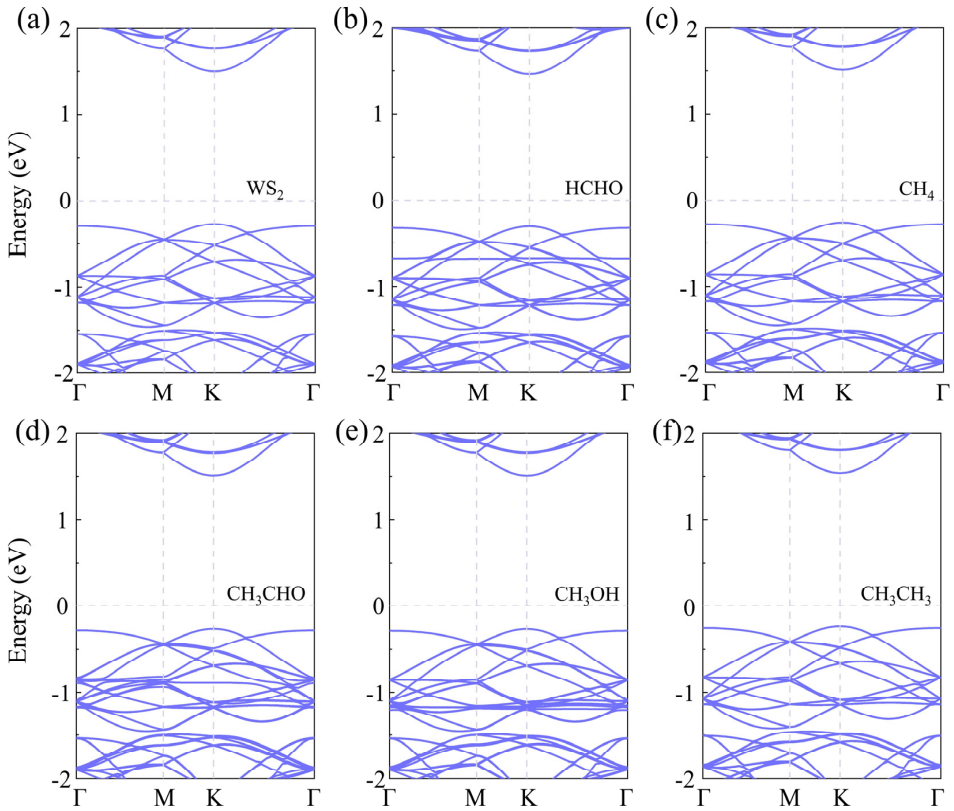

Figure 2. The band of (**a**) WS_2, (**b**) HCHO-WS_2, (**c**) CH_4-WS_2, (**d**) CH_3CHO-WS_2, (**e**) CH_3OH-WS_2, and (**f**) CH_3CH_3-WS_2.

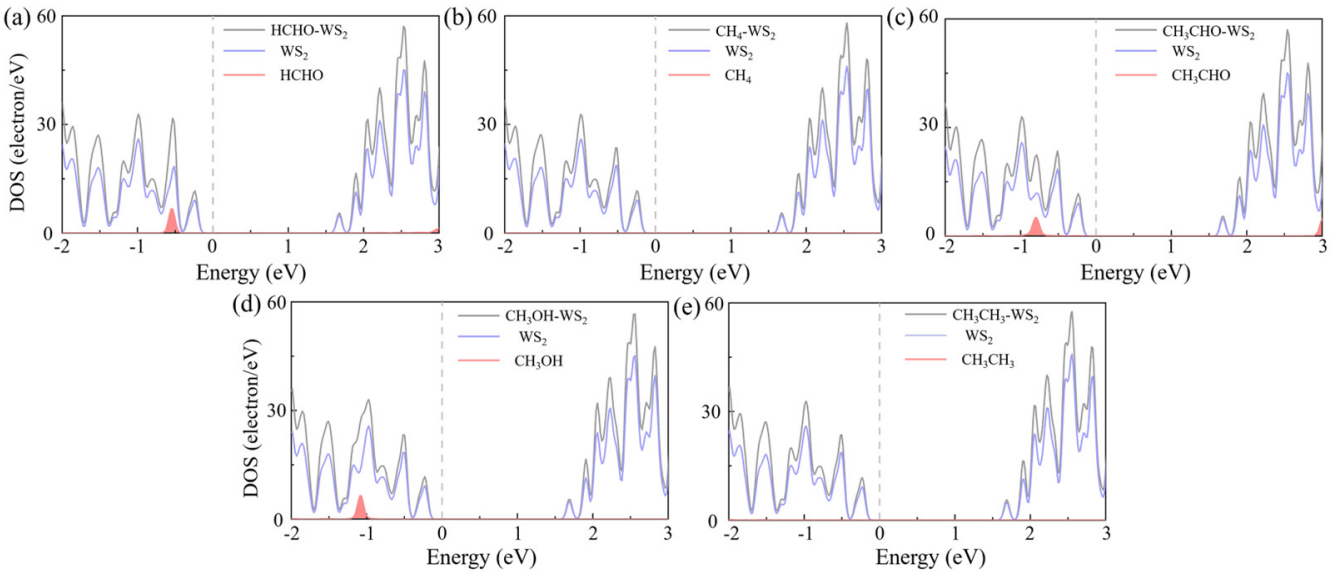

Figure 3. The DOS of (**a**) HCHO, (**b**) CH_4, (**c**) CH_3CHO, (**d**) CH_3OH, and (**e**) CH_3CH_3 adsorbed on WS_2.

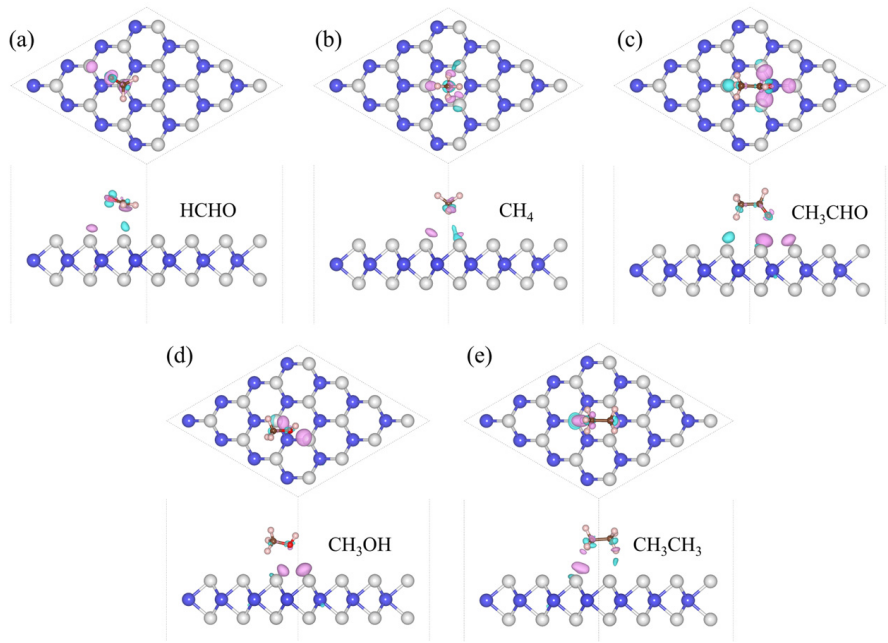

Figure 4. The CDD of (**a**) HCHO, (**b**) CH_4, (**c**) CH_3CHO, (**d**) CH_3OH, and (**e**) CH_3CH_3 adsorbed on WS_2 with the isosurface value of 3×10^{-4} e Å^{-1}. The W and S atoms are colored in blue and grey, the sky-blue area denotes the accumulation of electrons, and the purple area denotes the depletion of electrons.

An important research object in the study of 2D materials is vacancy defects. By adding vacancy defects in certain ways, scientists can investigate how defects affect electrical conductivity, optical absorption, electronic structure, and other aspects. Researchers can gain a deeper understanding of the relationship between a material's structure and properties, as well as expand the potential applications of 2D materials in areas like catalysis, sensing, and electrical devices through vacancy defects. Based on the WS_2 model, we removed the W atom to construct V_W/WS_2, and similarly removed the S atom to construct S defect WS_2 (V_S/WS_2), the model diagram of which is displayed in Figure 5a. Next, we computed the E_{ad} of these two structures after fully relaxing them. The E_{ad} of V_W/WS_2 is −17.33 eV, and that of V_S/WS_2 is −7.15 eV, as Figure 5b illustrates. We decided to focus our subsequent

research on V_W/WS_2 since the more negative adsorption energy it has, the more stable it becomes [36]. To gain more insight into this structure's thermal stability, we computed the ab initio molecular dynamics (AIMD) at 300 K [37–39]. V_W/WS_2 exhibits thermal stability, as evidenced by Figure 6b, where the total energy tends to stabilize across the simulation duration and the crystal structure is free of deformation and bond breaking. We computed the band structure [3] and DOS of V_W/WS_2 in order to comprehend its electronic properties. V_W/WS_2 is a direct band gap semiconductor with a band gap value of 0.379 eV, as can be seen in the band diagram in Figure 6c. The Fermi level is situated between the conduction band and the valence band, V_W/WS_2 is a semiconductor, and the 4f level of the W atom supplies the valence band maximum and conduction band minimum, which correlates to the energy band, as can be seen in the DOS diagram of Figure 6d.

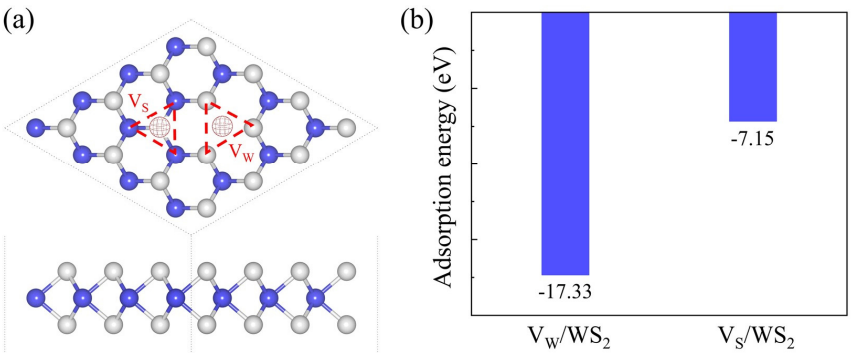

Figure 5. The (**a**) configuration and (**b**) adsorption energy of V_W/WS_2 and V_S/WS_2, the W and S atoms are colored in blue and grey.

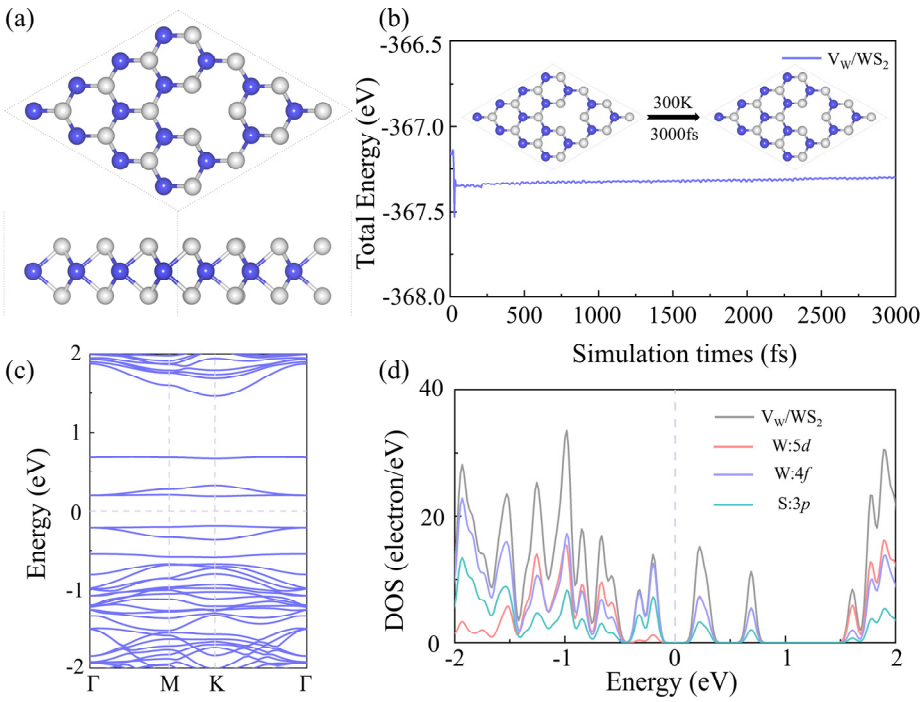

Figure 6. The (**a**) configuration, (**b**) graph of total energy and simulation time, (**c**) band structure, and (**d**) DOS of V_W/WS_2, the W and S atoms are colored in blue and grey.

The *H* of the adsorption systems before optimization is 3 Å. In Table 2, the most stable model (the *H* values are 2.92 Å, 2.79 Å, 2.65 Å, 2.67 Å, and 2.51 Å, respectively) for V_W/WS_2 to adsorb the five toxic gases—HCHO, CH_4, CH_3CHO, CH_3OH, and CH_3CH_3—is depicted in Figure 7 [11,40]. The band gap values of V_W/WS_2 and the five adsorption systems

are displayed in Figure 8 [41]. We can see that compared with V_W/WS_2 the band gap undergoes certain changes after adsorbing gas molecules. The DOSs of adsorption systems are displayed in Figure 9. Compared with other gas molecules, due to the structure and electronic configuration of HCHO, its oxygen atom may introduce more electrons, and some special electronic states may be introduced near the Fermi level, resulting in the formation of a local electronic state near the Fermi level. The DOS of HCHO is closer to the Fermi level and its contribution is greater near the Fermi level. The DOSs of CH_4 and CH_3CH_3 disappear near Fermi level, while the DOSs of CH_3CHO and CH_3OH are far away from Fermi level and their contribution is smaller. Therefore, V_W/WS_2 has high sensitivity and selectivity for HCHO. The CDD of the adsorption systems is shown in Figure 10. We can see the accumulation and dissipation of charge in the adsorption systems, which shows that the conductivity of V_W/WS_2 has changed to some extent after adsorbing gas molecules. In order to describe which gas molecules V_W/WS_2 is most sensitive to, we calculated *B*. As shown in Table 2, HCHO-V_W/WS_2 has the highest *B*, which shows that the conductivity of HCHO-V_W/WS_2 has the most obvious change, and V_W/WS_2 has high sensitivity and selectivity to HCHO [12,41–43].

Table 2. The E_{ad}, *H*, E_g, and *B* for HCHO, CH_4, CH_3CHO, CH_3OH, and CH_3CH_3 adsorbed on V_W/WS_2.

Configuration	E_{ad} (meV)	*H* (Å)	E_g (eV)	*B* (e)	*W* (eV)	Δ*W* (eV)
V_W/WS_2	-	-	0.379	-	5.432	-
HCHO-V_W/WS_2	−207.8	2.92	0.340	0.104	5.637	0.205
CH_4-V_W/WS_2	−144.5	2.79	0.341	−0.011	5.437	0.005
CH_3CHO-V_W/WS_2	−188.2	2.65	0.373	0.090	4.993	−0.439
CH_3OH-V_W/WS_2	−207.9	2.67	0.372	0.087	5.069	−0.363
CH_3CH_3-V_W/WS_2	−236.9	2.51	0.367	−0.016	5.440	0.008

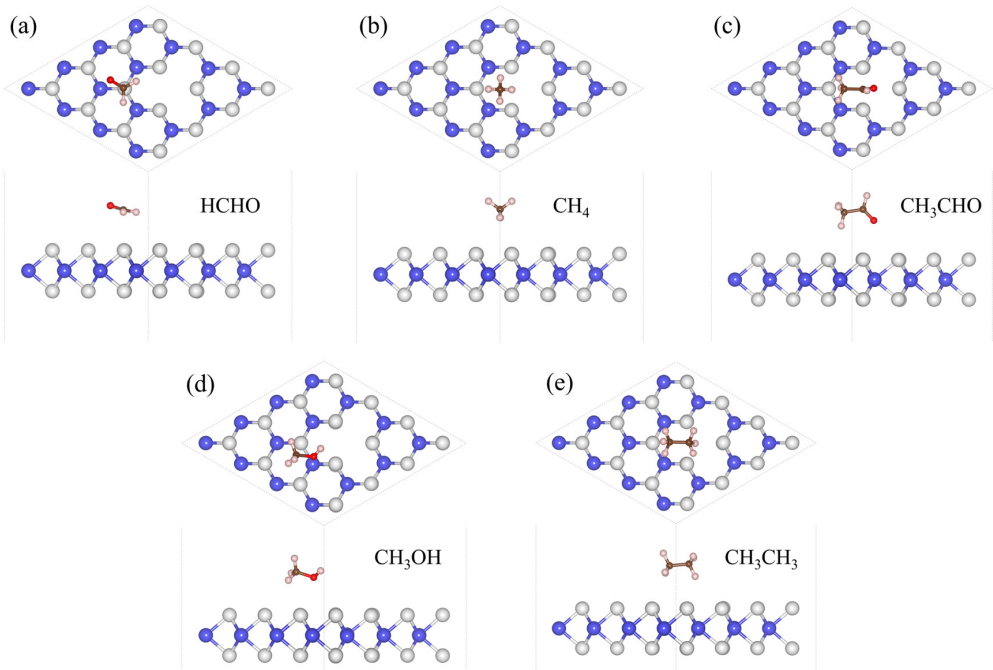

Figure 7. The most stable adsorption configurations of (**a**) HCHO, (**b**) CH_4, (**c**) CH_3CHO, (**d**) CH_3OH, and (**e**) CH_3CH_3 adsorbed on V_W/WS_2, the W and S atoms are colored in blue and grey.

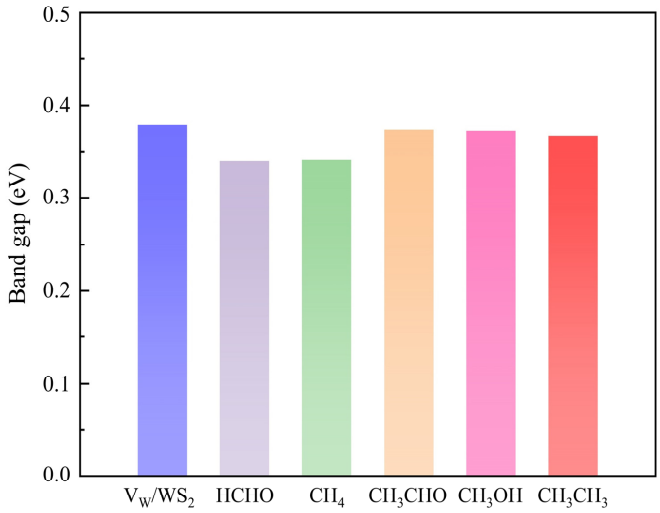

Figure 8. The band gap of HCHO, CH_4, CH_3CHO, CH_3OH, and CH_3CH_3 adsorbed on V_W/WS_2.

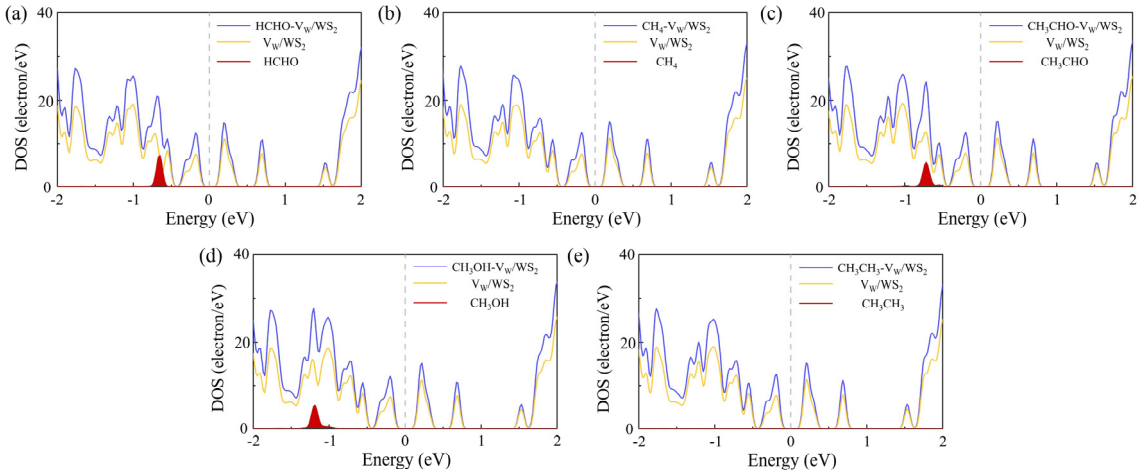

Figure 9. The DOS of (**a**) HCHO, (**b**) CH_4, (**c**) CH_3CHO, (**d**) CH_3OH, and (**e**) CH_3CH_3 adsorbed on V_W/WS_2.

The relationship between *W* and the sensitivity of chemical sensors is mainly reflected in the change in electronic structure caused by the interaction between materials and target molecules. This relationship is very important for understanding the working mechanism of the sensor, optimizing the sensor's performance, and designing a more selective and sensitive sensor. Additionally, we computed the *W* of five adsorption systems and the V_W/WS_2 [44]. ΔW represents the change in the *W* after adsorption, as seen in Table 2. The ΔW of the CH_4-V_W/WS_2 (0.005 eV) and CH_3CH_3-V_W/WS_2 (0.008 eV) systems show a minor increase, and the CH_3HO-V_W/WS_2 and CH_3OH-V_W systems show a decrease [45,46]. The *W* clearly increases for the HCHO-V_W/WS_2 system, and the change value is 0.205 eV, which is noticeably larger than for other adsorption systems. This indicates that V_W/WS_2 has high sensitivity and selectivity for HCHO and that HCHO will interact with V_W/WS_2 more readily when it is in contact with experimental gas. Device models can be used to predict the performance of electronic devices, including I–V characteristic, power consumption, and speed [47]. We constructed device models, as Figure 11a illustrates. The gadget is separated into a center scattering zone and left and right electrodes. The buffer layer can adjust the charge distribution in the device and prevent excessive charge from accumulating in a certain area, thus maintaining the stability and reliability of the device. The buffer layer can also block the diffusion of external impurities, protect the internal purity of the device, and reduce the negative impact on the performance of the device, so, at

the intersection of the electrodes and the central scattering region, we inserted three buffer layers to prevent any interference of the device center [48]. We utilized Materials studio software to compute the I–V characteristic of five adsorption systems and V_W/WS_2, which were represented by the I–V curve, so that we could clearly see the change in conductivity. The I–V curve is displayed in Figure 11b–f, where the gray lines in each figure correspond to the V_W/WS_2 I–V curve. We can observe that the current starts to increase when a bias voltage of 1.8 V is applied [49]. Compared with the I–V curve of BC_6N adsorption systems [33], the slope change of the I–V curve after V_W/WS_2 adsorbed gas molecules is more obvious, and the conductivity change is more sensitive when detecting gas molecules. Figure 11b shows us that hardly any current passes through HCHO-V_W/WS_2 when the bias voltage is less than 1.8 V. The current increases dramatically when the applied bias voltage rises above the threshold value (1.8 V). The current of 1.14×10^{-7} A is reached at 2.4 V, which is much greater than that of V_W/WS_2 (7.99×10^{-8} A). Following adsorption, V_W/WS_2 is clearly sensitive to HCHO, as seen by the sharply altered I–V curve, higher slope (under the bias voltage of 1.8 V~2.4 V), and clearly increased conductivity. The I–V curves of the four types of adsorption systems in Figure 11c–f have altered somewhat when compared to the I–V curve of the V_W/WS_2. By examining the slope, we can also observe that V_W/WS_2 has the maximum sensitivity to HCHO, as seen by the I–V curves of the five adsorption systems (which is compatible with the *W* calculation results). It can also demonstrate the selectivity of the sensor, allowing us to differentiate HCHO from other gases through the observation of the conductivity shift. To validate the work function and I–V curve results, we computed V_W/WS_2 sensitivity at 1.8 V, 2.0 V, 2.2 V, and 2.4 V bias voltages [50,51]. Table 3 displays the results of the calculation [52]. The sensitivity of V_W/WS_2 to HCHO, CH_4, CH_3HO, CH_3OH, and CH_3CH_3 is 98.1%, 96.7%, 88.9%, 94.9%, and 96.0%, respectively, when a bias voltage of 1.8 V is applied to the adsorption systems. This indicates that V_W/WS_2 has high sensitivity to these five gases at a voltage of 1.8 V. The sensitivity of Pt-NiS_2 to HCHO is −99.2% [53], and the sensitivity of V_W/WS_2 to HCHO is −98.1% under 1.8 V, so it is necessary to study further. Significantly higher than that of other adsorbed gas molecules, the sensor's sensitivity to HCHO is 108.0% and 42.9% at 2.2 V and 2.4 V, respectively [54–56]. This suggests that V_W/WS_2 can selectively detect HCHO, and the calculated results are in agreement with those of *W* and the I–V characteristic.

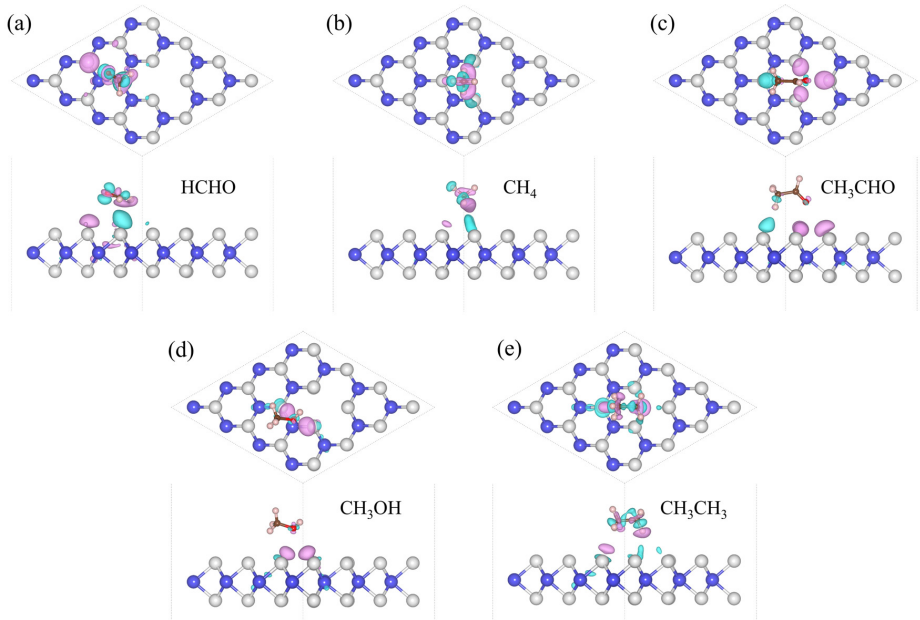

Figure 10. The CDD of (**a**) HCHO, (**b**) CH_4, (**c**) CH_3CHO, (**d**) CH_3OH, and (**e**) CH_3CH_3 adsorbed on V_W/WS_2. The W and S atoms are colored in blue and grey, the sky-blue area denotes the accumulation of electrons, and the purple area denotes the depletion of electrons. The value of the isosurface is set to 3×10^{-4} e Å^{-1}.

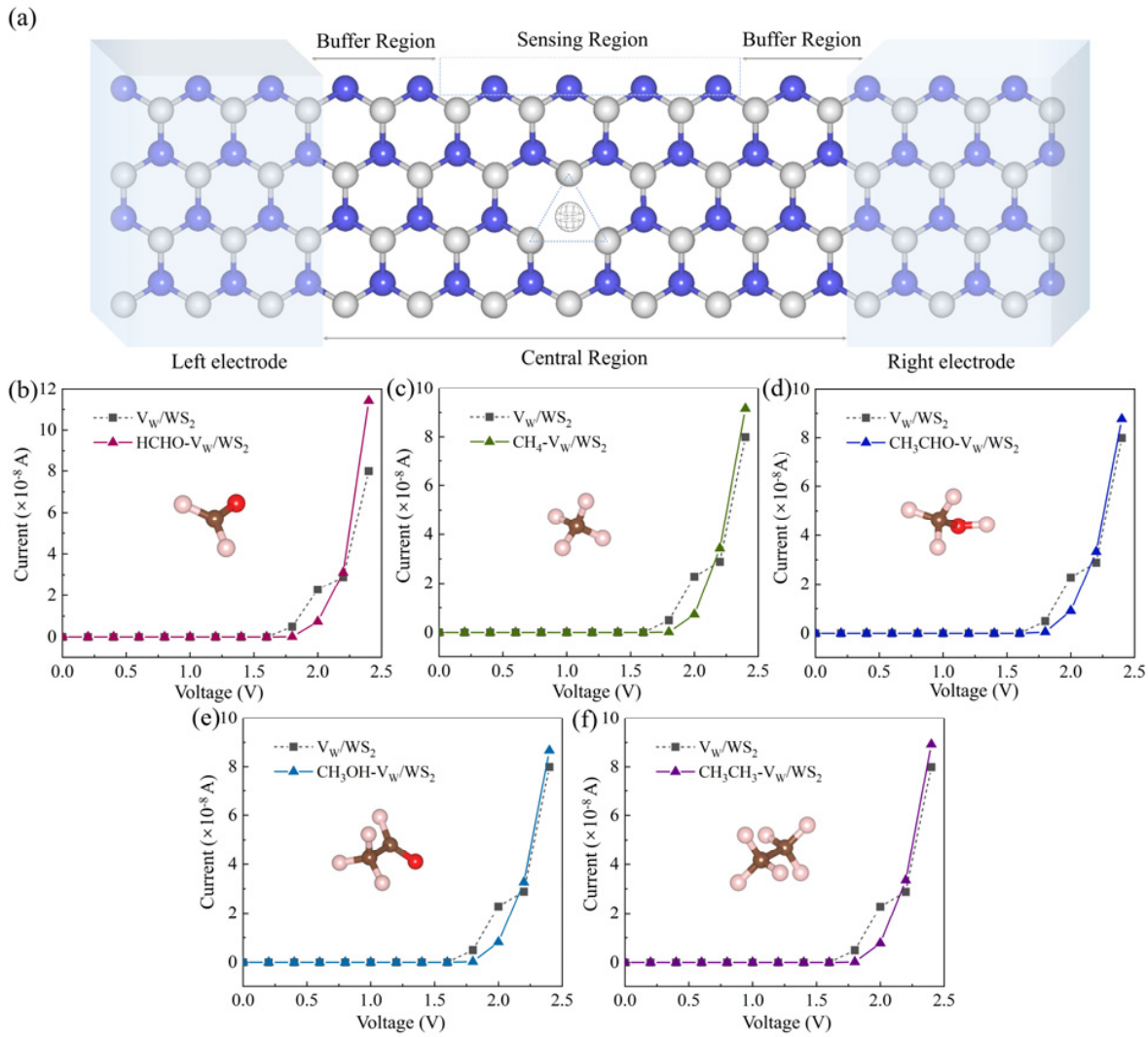

Figure 11. Device model for V_W/WS_2 adsorption systems of (**a**) and the I–V curve of (**b**) HCHO, (**c**) CH_4, (**d**) CH_3CHO, (**e**) CH_3OH, and (**f**) CH_3CH_3 adsorbed on V_W/WS_2.

Table 3. The sensitivity (%) of the sensor based on V_W/WS_2 with left and right electrodes toward HCHO, CH_4, CH_3CHO, CH_3OH, and CH_3CH_3 at bias voltage of 1.8 V, 2.0 V, 2.2 V, and 2.4 V. Negative (positive) sensitivity means that the current of the sensor dropped (enhanced) after interaction with the adsorption.

Bias Voltage (V)	HCHO	CH_4	CH_3CHO	CH_3OH	CH_3CH_3
1.8	−98.1	−96.7	−88.9	−94.9	−96.0
2.0	−67.7	−67.9	−60.0	−64.1	−65.8
2.2	+108.0	+18.9	+15.3	+13.2	+16.2
2.4	+42.9	+14.6	+9.75	+8.46	+11.7

4. Conclusions

This research uses a series of simulations to study the gas sensitivity of V_W/WS_2 to HCHO, CH_4, CH_3HO, CH_3OH, and CH_3CH_3. Initially, we used first-principles calculations to determine the system's electronic properties. According to the DOS, HCHO contributes more than other gas molecules to an energy level close to the Fermi level. The HCHO-V_W/WS_2 *B* is the biggest (0.104 e). The system's *W* was then computed, and the HCHO system's *W* clearly rose. We also calculated the I–V characteristic. It was observed that in the case of adsorbed HCHO, the corresponding conductivity increased most dramatically

and the slope increased most noticeably once the bias voltage rose beyond the threshold voltage. Therefore, V_W/WS_2 can solve the cross-sensitivity and other defects of general chemical sensors, and then develop into HCHO chemical sensors with high sensitivity and selectivity, which can be further integrated into flexible wearable devices to realize real-time monitoring of individual health and environmental factors.

Author Contributions: Z.C.: Supervision, Writing—review & editing. H.W.: Conceptualization, Writing—original draft, Methodology. K.Y.: Data curation Y.S.: Software, Validation. K.Q.: Data curation. P.Y.: Data curation. E.L.: Supervision, Writing-review & editing. All authors have read and agreed to the published version of the manuscript.

Funding: This work was funded by the National Natural Science Foundation of China (No. 12104362), the Natural Science Basic Research Plan in Shaanxi Province of China (Program No. 2021JM-345), the China Postdoctoral Science Foundation (Program No. 2020M683684XB), and the Shaanxi Province Innovative Talents Promotion Plan-Young Science and Technology Star Project (No. 2022KJXX-61).

Institutional Review Board Statement: Not applicable.

Informed Consent Statement: Not applicable.

Data Availability Statement: Data are contained within the article.

Acknowledgments: We gratefully acknowledge HZWTECH for providing the computation facilities and thank Xiaowen Shi (from HZWTECH) for the help and discussions regarding this study.

Conflicts of Interest: The authors declare that they have no known competing financial interests or personal relationships that could have appeared to influence the work reported in this paper.

References

1. Li, X.; Wu, S.; Wang, F.; You, L.; Yang, C.; Cui, P.; Zhang, X. Quantitative assessments of GHG and VOCs emissions of asphalt pavement contained steel slag. *Constr. Build. Mater.* **2023**, *369*, 130606. [CrossRef]
2. Cui, Z.; Liu, D.; Zhu, W.; Zhang, S.; Wang, L. A tunable terahertz broadband absorber based on patterned vanadium dioxide. *Micro Nanostruct.* **2024**, *186*, 207734. [CrossRef]
3. Sun, M.; Re Fiorentin, M.; Schwingenschlögl, U.; Palummo, M. Excitons and light-emission in semiconducting $MoSi_2X_4$ two-dimensional materials. *NPJ 2d Mater. Appl.* **2022**, *6*, 81. [CrossRef]
4. Yuan, J.; Wei, Q.; Sun, M.; Yan, X.; Cai, Y.; Shen, L.; Schwingenschlögl, U. Protected valley states and generation of valley- and spin-polarized current in monolayer. *Phys. Rev. B* **2022**, *105*, 195151. [CrossRef]
5. Cui, Z.; Wu, H.; Yang, K.; Wang, X.; Lv, Y. Adsorption of gas molecules on intrinsic and defective $MoSi_2N_4$ monolayer: Gas sensing and functionalization. *Sens. Actuators A Phys.* **2024**, *366*, 114954. [CrossRef]
6. Acharyya, S.; Nag, S.; Guha, P.K. Ultra-selective tin oxide-based chemiresistive gas sensor employing signal transform and machine learning techniques. *Anal. Chim. Acta* **2022**, *1217*, 339996. [CrossRef] [PubMed]
7. Papaconstantinou, R.; Demosthenous, M.; Bezantakos, S.; Hadjigeorgiou, N.; Costi, M.; Stylianou, M.; Symeou, E.; Savvides, C.; Biskos, G. Field Evaluation of Low-cost Electrochemical Air Quality Gas Sensors at Extreme Temperature and Relative Humidity Conditions. *EGUsphere* **2023**, *2023*, 3313–3329. [CrossRef]
8. Khan, M.A.; Rao, M.V.; Li, Q. Recent Advances in Electrochemical Sensors for Detecting Toxic Gases: NO_2, SO_2 and H_2S. *Sensors* **2019**, *19*, 905. [CrossRef]
9. Xu, R.; Kong, F.; Wan, J.; Guo, J. Computational evaluation of sensing properties of a novel 2D diboron dinitride for detecting toxic gas molecules. *Mater. Sci. Semicond. Process.* **2023**, *161*, 107446. [CrossRef]
10. Sohrabi, H.; Ghasemzadeh, S.; Ghoreishi, Z.; Majidi, M.R.; Yoon, Y.; Dizge, N.; Khataee, A. Metal-organic frameworks (MOF)-based sensors for detection of toxic gases: A review of current status and future prospects. *Mater. Chem. Phys.* **2023**, *299*, 127512. [CrossRef]
11. Cui, Z.; Yang, K.; Shen, Y.; Yuan, Z.; Dong, Y.; Yuan, P.; Li, E. Toxic gas molecules adsorbed on intrinsic and defective WS_2: Gas sensing and detection. *Appl. Surf. Sci.* **2023**, *613*, 155978. [CrossRef]
12. Li, T.; Miao, Q.; Wang, Y.; Yang, H. 2D NbS_2 monolayer as a gas sensor for the detection of nitrogen-containing toxic gases. *Surf. Interfaces* **2023**, *42*, 103336. [CrossRef]
13. Xu, H.; Zhang, J.; Rehman, A.U.; Gong, L.; Kan, K.; Li, L.; Shi, K. Synthesis of NiO@CuO nanocomposite as high-performance gas sensing material for NO_2 at room temperature. *Appl. Surf. Sci.* **2017**, *412*, 230–237. [CrossRef]
14. Zhang, C.; Ren, K.; Wang, S.; Luo, Y.; Tang, W.; Sun, M. Recent progress on two-dimensional van der Waals heterostructures for photocatalytic water splitting: A selective review. *J. Phys. D Appl. Phys.* **2023**, *56*, 483001. [CrossRef]
15. Yang, K.; Cui, Z.; Li, E.; Shen, Y.; Zhang, L.; Ma, D.; Yuan, Z.; Dong, Y.; Zhang, S. Modulation of the magnetic, electronic, and optical behaviors of WS_2 after metals adsorption: A first-principles study. *Chem. Phys.* **2023**, *571*, 111903. [CrossRef]

16. Cui, Z.; Wang, H.; Shen, Y.; Qin, K.; Yuan, P.; Li, E. $MoSe_2$ and WSSe heterojunction with exceptional power conversion efficiency and photogalvanic effect. *Mater. Today Phys.* **2024**, *40*, 101317. [CrossRef]
17. Cong, C.; Shang, J.; Wang, Y.; Yu, T. Optical Properties of 2D Semiconductor WS_2. *Adv. Opt. Mater.* **2018**, *6*, 1700767. [CrossRef]
18. Poornimadevi, C.; Preferencial Kala, C.; John Thiruvadigal, D. First principle analysis of toxic gas adsorption on pristine WS_2 and Fe-doped WS_2: Implications for gas sensing. *Surf. Interfaces* **2023**, *42*, 103518. [CrossRef]
19. Poornimadevi, C.; Gayathri Devi, S.; Preferencial Kala, C.; Thiruvadigal, D.J. Ab Initio Study of Electronic Properties on WS_2 Monolayer and Transition Metal Doped WS2. *ECS J. Solid State Sci. Technol.* **2022**, *11*, 073003. [CrossRef]
20. Alam, M.M.; Asiri, A.M.; Uddin, J.; Rahman, M.M. Selective 1,4-dioxane chemical sensor development with doped ZnO/GO nanocomposites by electrochemical approach. *J. Mater. Sci. Mater. Electron.* **2022**, *33*, 4360–4374. [CrossRef]
21. Chen, X.P.; Wang, L.M.; Sun, X.; Meng, R.S.; Xiao, J.; Ye, H.Y.; Zhang, G.Q. Sulfur Dioxide and Nitrogen Dioxide Gas Sensor Based on Arsenene: A First-Principle Study. *IEEE Electron Device Lett.* **2017**, *38*, 661–664. [CrossRef]
22. Miao, J.; Yu, C.; Xia, J.; Xue, Z.; Li, X.; Dai, M.; Heng, Y.; Jiang, D.; Li, Q. New NASICON-based all-solid-state reference electrode towards a pH sensor for the electrochemical measurement of harsh environments. *Ionics* **2022**, *28*, 2437–2445. [CrossRef]
23. Chen, A.; Wu, W.; Fegley, M.E.A.; Pinnock, S.S.; Duffy-Matzner, J.L.; Bernier, W.E.; Jones, W.E. Pentiptycene-Derived Fluorescence Turn-Off Polymer Chemosensor for Copper(II) Cation with High Selectivity and Sensitivity. *Polymers* **2017**, *9*, 118. [CrossRef] [PubMed]
24. Jin, J.-C.; Wu, J.; Yang, G.-P.; Wu, Y.-L.; Wang, Y.-Y. A microporous anionic metal–organic framework for a highly selective and sensitive electrochemical sensor of Cu^{2+} ions. *Chem. Commun.* **2016**, *52*, 8475–8478. [CrossRef] [PubMed]
25. Yang, Y.; Liu, S.; Shi, P.; Zhao, G. A Highly Sensitive and Selective Label-free Electrochemical Biosensor with a Wide Range of Applications for Bisphenol A Detection. *Electroanalysis* **2022**, *34*, 743–751. [CrossRef]
26. James, T.E.; Hemmingson, S.L.; Sellers, J.R.V.; Campbell, C.T. Calorimetric measurement of adsorption and adhesion energies of Cu on Pt(111). *Surf. Sci.* **2017**, *657*, 58–62. [CrossRef]
27. Men'shchikov, I.E.; Fomkin, A.A.; Shkolin, A.V.; Strizhenov, E.M.; Zaitsev, D.S.; Tvardovskii, A.V. The energy of adsorption of methane on microporous carbon adsorbents. *Prot. Met. Phys. Chem. Surf.* **2017**, *53*, 780–785. [CrossRef]
28. Cui, Z.; Wu, H. Metal atoms adsorbed Ga_2O_3 monolayer: As a potential application in optoelectronic devices. *Micro Nanostruct.* **2023**, *180*, 207613. [CrossRef]
29. Cui, Z.; Yang, K.; Ren, K.; Zhang, S.; Wang, L. Adsorption of metal atoms on $MoSi_2N_4$ monolayer: A first principles study. *Mater. Sci. Semicond. Process.* **2022**, *152*, 107072. [CrossRef]
30. Kempfer-Robertson, E.M.; Haase, M.N.; Bersson, J.S.; Avdic, I.; Thompson, L.M. Role of Exact Exchange in Difference Projected Double-Hybrid Density Functional Theory for Treatment of Local, Charge Transfer, and Rydberg Excitations. *J. Phys. Chem. A* **2022**, *126*, 8058–8069. [CrossRef]
31. Yoon, Y.; Zhang, Z.; Qi, R.; Joe, A.Y.; Sailus, R.; Watanabe, K.; Taniguchi, T.; Tongay, S.; Wang, F. Charge Transfer Dynamics in $MoSe_2$/hBN/WSe_2 Heterostructures. *Nano Lett.* **2022**, *22*, 10140–10146. [CrossRef] [PubMed]
32. Paul, F.; Nama Manjunatha, K.; Paul, S. Non-Zero and Open-Loop Current–Voltage Characteristics in Electronic Memory Devices. *Adv. Electron. Mater.* **2023**, *9*, 2300324. [CrossRef]
33. Aghaei, S.M.; Aasi, A.; Farhangdoust, S.; Panchapakesan, B. Graphene-like BC6N nanosheets are potential candidates for detection of volatile organic compounds (VOCs) in human breath: A DFT study. *Appl. Surf. Sci.* **2021**, *536*, 147756. [CrossRef]
34. Taylor, J.; Guo, H.; Wang, J. Ab initio modeling of quantum transport properties of molecular electronic devices. *Phys. Rev. B* **2001**, *63*, 245407. [CrossRef]
35. Waldron, D.; Haney, P.; Larade, B.; MacDonald, A.; Guo, H. Nonlinear Spin Current and Magnetoresistance of Molecular Tunnel Junctions. *Phys. Rev. Lett.* **2006**, *96*, 166804. [CrossRef] [PubMed]
36. Qi, C.; Xu, X.; Chen, J.; Guo, L.; Chen, Q. Ab initio calculations of CO2 adsorption on β-C2S(100) and M3-C3S(001) surfaces: An exploration of early CO_2 sequestration pathways. *Environ. Res.* **2022**, *215*, 114412. [CrossRef] [PubMed]
37. Li, J.; Zhang, H.; Guo, Z.; Jiang, J.-W.; Chang, T. Thermal stability of twin graphene: A Reaxff molecular dynamics study. *Appl. Surf. Sci.* **2023**, *623*, 157038. [CrossRef]
38. Zhang, W.; Chai, C.; Fan, Q.; Yang, Y.; Sun, M.; Palummo, M.; Schwingenschlögl, U. Two-dimensional borocarbonitrides for photocatalysis and photovoltaics. *J. Mater. Chem. C* **2023**, *11*, 3875–3884. [CrossRef]
39. Ren, K.; Yan, Y.; Zhang, Z.; Sun, M.; Schwingenschlögl, U. A family of LixBy monolayers with a wide spectrum of potential applications. *Appl. Surf. Sci.* **2022**, *604*, 154317. [CrossRef]
40. Osborne, D.A.; Morishita, T.; Tawfik, S.A.; Yayama, T.; Spencer, M.J.S. Adsorption of toxic gases on silicene/Ag(111). *Phys. Chem. Chem. Phys.* **2019**, *21*, 17521–17537. [CrossRef]
41. Meshginqalam, B.; Barvestani, J. Highly sensitive toxic gas molecule sensor based on defect-induced silicene. *J. Mater. Sci. Mater. Electron.* **2019**, *30*, 18637–18646. [CrossRef]
42. Kang, M.; Liu, T.; Sun, H.; Li, L.; Wang, K. Blue phosphorus phase GeSe monolayer for nitrogenous toxic gas sensing: A DFT study. *Sens. Actuators A Phys.* **2024**, *365*, 114861. [CrossRef]
43. Godbole, R.; Godbole, V.P.; Bhagwat, S. Surface morphology dependent tungsten oxide thin films as toxic gas sensor. *Mater. Sci. Semicond. Process.* **2017**, *63*, 212–219. [CrossRef]
44. Yang, Y.; Sun, Y.; Luo, C.; Fu, Q.; Pan, C. Effect of metal's inherent characteristics on sensibility of flexible metal-based composite sensor and its applications. *Sens. Actuators A Phys.* **2021**, *327*, 112754. [CrossRef]

45. Kumar, P.; Gupta, M.; Singh, K.; Kumar, N. Analysis of transition metal dichalcogenides materials based gas sensor using non-equilibrium green's function. *Int. J. Numer. Model. Electron. Netw. Devices Fields* **2023**, *36*, e3036. [CrossRef]
46. Gardner, D.W.; Gao, X.; Fahad, H.M.; Yang, A.-T.; He, S.; Javey, A.; Carraro, C.; Maboudian, R. Transistor-Based Work-Function Measurement of Metal–Organic Frameworks for Ultra-Low-Power, Rationally Designed Chemical Sensors. *Chem. A Eur. J.* **2019**, *25*, 13176–13183. [CrossRef] [PubMed]
47. Jung, S.-W.; Shin, M.-C.; Schweitz, M.A.; Oh, J.-M.; Koo, S.-M. Influence of Gas Annealing on Sensitivity of AlN/4H-SiC-Based Temperature Sensors. *Materials* **2021**, *14*, 683. [CrossRef]
48. Rahman, M.M.; Ahmed, J.; Asiri, A.M.; Siddiquey, I.A.; Hasnat, M.A. Development of 4-methoxyphenol chemical sensor based on NiS_2-CNT nanocomposites. *J. Taiwan Inst. Chem. Eng.* **2016**, *64*, 157–165. [CrossRef]
49. Sharma, S.; Tiwari, M.; Nurbash, S.V.; Gagrani, R.; Bhuin, S.; Chappanda, K.N. Enhancement in TiO2 Nanotubes Based Electrochemical Sensors via Synergistic Effect of $TiCl_4$ Surface Engineering. *IEEE Sens. J.* **2022**, *22*, 33–41. [CrossRef]
50. Yao, P.-C.; Niu, J.-S.; Dai, G.-Y.; Jian, J.-J.; Hsu, W.-C.; Lin, K.-W.; Liu, W.-C. Ammonia sensing characteristics of an ITO-V2O5 based chemoresistive dual-type gas sensors (CDGS) decorated with platinum nanoparticles. *Sens. Actuators B Chem.* **2023**, *392*, 134071. [CrossRef]
51. Rajapaksha, R.D.A.A.; Hashim, U.; Gopinath, S.C.B.; Fernando, C.A.N. Sensitive pH detection on gold interdigitated electrodes as an electrochemical sensor. *Microsyst. Technol.* **2018**, *24*, 1965–1974. [CrossRef]
52. Jung, G.; Hong, S.; Shin, W.; Jeong, Y.; Park, J.; Kim, D.; Lee, J.-H. Design optimization of FET-type gas sensor considering device characteristics, sensitivity, power, noise, and SNR. *Sens. Actuators B Chem.* **2022**, *369*, 132257. [CrossRef]
53. Li, S.; He, J.; Man, Y.; Li, L.; Li, S.; Li, N.; Zhao, Q. A first-principles study into Pt-embedded NiS_2 monolayer as an outstanding gas sensor upon CO and HCHO dry-type reactors. *Comput. Theor. Chem.* **2023**, *1226*, 114203. [CrossRef]
54. Opoku, F.; Govender, P.P. Two-dimensional CoOOH as a Highly Sensitive and Selective H2S, HCN and HF Gas Sensor: A Computational Investigation. *Electroanalysis* **2020**, *32*, 2764–2774. [CrossRef]
55. Singh, A.; Yadav, B.C. Photo-responsive highly sensitive CO_2 gas sensor based on SnO_2@CdO heterostructures with DFT calculations. *Surf. Interfaces* **2022**, *34*, 102368. [CrossRef]
56. Jiang, T.; He, Q.; Bi, M.; Chen, X.; Sun, H.; Tao, L. First-principles calculations of adsorption sensitivity of Au-doped MoS_2 gas sensor to main characteristic gases in oil. *J. Mater. Sci.* **2021**, *56*, 13673–13683. [CrossRef]